Unmixed Zone Formation in Austenitic Stainless Steel Weldments

"Fully" austenitic weldments may exhibit an increased susceptibility to stress-corrosion cracking as the result of a duplex austenite-ferrite microstructure at the weld interface

BY W. A. BAESLACK, III, J. C. LIPPOLD AND W. F. SAVAGE

ABSTRACT. An investigation of the weld interface region in heterogeneous austenitic stainless steel weldments on an 18Cr-8Ni base metal indicates that a well-developed unmixed zone exists along the boundary separating the weld composite region from the partially-melted region. Since the unmixed zone exists as a laminar layer of base metal which has melted and resolidified *in situ* during the welding process, the average composition of this region is identical to that of the base metal. In addition, the duplex austenite-ferrite microstructure of the unmixed zone appears similar morphologically to the microstructure of autogenous 18Cr-8Ni weldments.

Constant extension rate stress-corrosion cracking tests were performed on transverse-welded tensile specimens in room and elevated temperature chloride-containing solutions which readily produce stress-corrosion cracking in 18Cr-8Ni base materials. Test results indicate that the duplex unmixed zone can be preferentially susceptible to corrosion-induced attack. Preferential environmentally-induced cracking in the unmixed zone of both Type 310/Type 304L and Type 312/Type 304L weldments is particularly severe in low pH, room temperature solutions; it involves the combined and interrelated occurrence of stress-assisted ferrite dissolution and stress-corrosion cracking in the austenite.

Thus, designing a "wholly" austenitic weldment by simply using a high-nickel filler metal is not possible. It could lead to catastrophic results if such weldments are employed under conditions conducive to stress-corrosion cracking.

Introduction

The wide application of 18Cr-8Ni austenitic stainless steels by the power and chemical industries has promoted a considerable interest in stainless steel weldments. As a result, substantial work has been performed to develop wholly-austenitic and duplex austeno-ferritic stainless steel weld metals with improved weldability and optimum mechanical properties and which provide adequate corrosion resistance.

Unfortunately, most of these studies have been founded on the classical premise that a weldment consists of weld metal (that portion of the weld which was entirely molten) bounded at the fusion line by a heat-affected zone (that portion of the base metal which was not melted, but which underwent thermally-induced microstructural changes during welding). This rather simplistic view of weld structure assumes that a distinct, two-dimensional boundary separates the weld metal from the heat-affected zone. Despite the obvious convenience of this assumption, studies by Savage *et al.*[1] have shown that on a microscopic scale the microstructure is not nearly so simple, and that the fusion boundary is not a clearly-defined "fusion line."

The schematic illustration in Fig. 1, from the work of Savage, shows that a heterogenous weld is actually comprised of four regions: a composite region, an unmixed zone, a partially-melted region, and a "true" heat-affected zone. In the composite region, hydrodynamic mixing of the molten filler and base metals results in a relatively uniform chemical composition; this in turn is separated by a diffusion gradient from the unmixed zone where a small portion of the base metal totally melts and resolidifies without undergoing filler metal dilution. The outer edge of the unmixed zone bounds a partially-melted region at the weld interface.

Constitutional liquation and grain boundary wetting in the partially-melted region result in various degrees of base metal melting. Outside of the partially-melted region a "true" heat-affected zone exists, where thermally-induced, solid-state changes in the base metal microstructure occur.

Objectives

The weld fusion boundary in heterogeneous weldments on 18Cr-8Ni stainless steels is clearly complex. Formation of the duplex partially-melted and "true" heat-affected zone regions involves the interrelated and simultaneous occurrence of several metallurgical phenomena. It is this complex nature which has prevented the observation of an unmixed zone in these weldments. Accordingly, the objectives of this study were two-

Paper presented at the AWS 60th Annual Meeting held in Detroit, Michigan, during April 2-6, 1979.

W. A. BAESLACK, III, and J. C. LIPPOLD were Graduate Fellows at R.P.I. and are now, respectively, with the Air Force Materials Laboratory, Wright Patterson Air Force Base, Ohio, and Sandia Laboratories, Livermore, California; W. F. SAVAGE is Professor of Metallurgical Engineering and Director of Welding Research, Rensselaer Polytechnic Institute, Troy, New York.

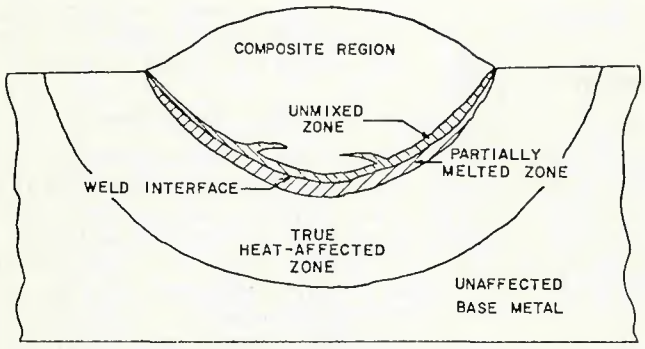

Fig. 1—Schematic illustration showing the regions of a heterogeneous weld

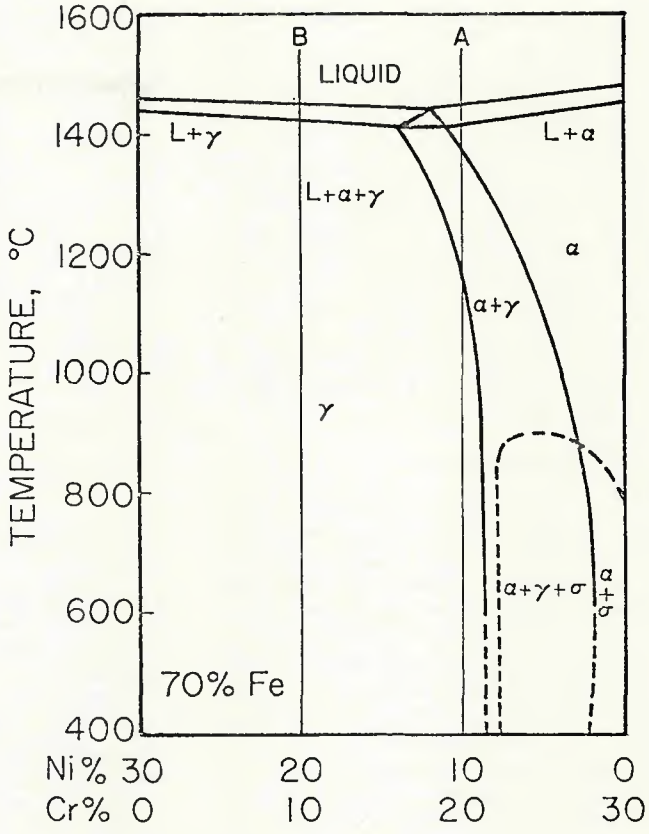

Fig. 2 (right)—Equilibrium Fe-Cr-Ni pseudo-binary diagram at 70 wt-% iron

fold:

1. To investigate unmixed zone formation and morphology in "wholly-austenitic" and "high-ferrite" weldments on 18Cr-8Ni stainless steel base metal,
2. To determine the importance of unmixed zone formation on the stress-corrosion cracking properties of stainless steel weldments.

Background

Investigations of the morphology and solidification of heterogeneous duplex stainless steel weldments have concentrated primarily on the composite region. Very little work has been concerned with the formation and morphology of the unmixed zone, the partially-melted region, or the "true" heat-affected zone. The following paragraphs briefly describe the formation and morphology of specific regions in heterogeneous weldments produced on wholly-austenitic 18Cr-8Ni base metals.

The Composite Region

By referring to an Fe-Cr-Ni pseudo-binary diagram, such as shown in Fig. 2 at 70% Fe, it is possible to predict the solidification sequence of a 20Cr-10Ni stainless steel.[2] Solidification under equilibrium conditions clearly occurs as primary ferrite. When the alloy is cooled slowly after solidification, a solid-state ferrite-to-austenite transformation takes place; this results in a fully austenitic room-temperature microstructure.

Savage et al.[3] have observed that nonequilibrium solidification and rapid cooling associated with the weldment composite region considerably alters solidification and solid-state transformation mechanics. They found that, although the composite region of an 18Cr-8Ni weldment solidifies as primary ferrite, nonequilibrium solidification forces the composition of the last-to-solidify liquid into the triangular three-phase region; this results in the formation of a divorced austenite-ferrite eutectic in the interdendritic regions.

By applying "Case III" nonequilibrium solidification principles* to the pseudo-binary phase diagram illustrated in Fig. 2, it can be shown that the initial ferrite which solidifies at the cores of the subgrains (dendrites) is so highly enriched in chromium that it remains ferritic after cooling to room temperature. The remainder of the subgrain solidifies at near-nominal composition until the impingement of adjacent dendrites results in the formation of the austenite-ferrite eutectic at the dendrite interstices. During subsequent cooling of the weldment, the austenite at the dendrite interstices consumes the primary ferrite of near-nominal composition in a diffusionless, massive-type reaction. As a result, the room temperature microstructure consists of a semi-continuous distribution of retained ferrite situated at the former dendrite cores. This vermicular morphology is typical in 18Cr-8Ni weld metals and is illustrated in Fig. 3.

Increasing the ratio of ferrite-stabilizing elements (Cr, Mo, Cb) to austenite-stabilizing elements (C, Mn, Ni) in the weld composite region results in greater quantities of retained ferrite and increasingly continuous ferrite networks. However, at ferrite levels greater than 20 vol-%, the vermicular duplex structure evolves into a structure consisting of blocky grains which exhibit a lathe-like mixture of austenite and ferrite and are surrounded by a continuous network of austenite. As the amount of ferrite-stabilizing elements is further increased, the alloy cools to room temperature entirely within the two-phase austenite plus ferrite region of the pseudo-binary diagram—Fig. 2. As a result, much of the ferrite transforms to austenite in a Widmanstatten precipitation reaction which is nucleated by the eutectic austenite at the grain and subgrain boundaries.

Increasing the quantity of austenite-stabilizing elements relative to the ferrite-stabilizing elements in the weld composite region promotes the solidification as primary austenite and results in less retained ferrite in the as-welded microstructure. Traverse B of the Fe-Cr-Ni pseudo-binary diagram, illustrated in Fig. 2, represents an

**In Case III solidification there is no diffusion in the solid and no mechanical mixing in the liquid. Concentration changes in the liquid occur by diffusion only. These boundary conditions can be shown to be closely approximated in most fusion welding processes.*

alloy which solidifies as primary austenite.

As in the composite regions which solidify as primary ferrite, nonequilibrium solidification associated with welding can permit the formation of an austenite-ferrite eutectic mixture as the composition of the last-to-solidify liquid is forced into the three-phase triangular region. This final liquid is highly enriched in chromium. As a result a large proportion of the eutectic ferrite remains stable to room temperature where it appears in a discontinuous distribution along grain and subgrain boundaries.

The Partially-Melted Region

The existence of a partially-melted zone (PMZ) in autogenous and heterogeneous weldments on wholly-austenitic 18Cr-8Ni stainless steels has been observed by several investigators.[3,4] Studies presently in progress at R.P.I. indicate that grain boundary and solute band liquation in the PMZ may involve the simultaneous occurrence of several phenomena.

Liquation of solute bands can result from the lower effective melting temperatures of these regions compared to that of the bulk of the microstructure. Work performed by Miller *et al.*[5] on 70Cu-30Ni weldments showed that the degree of solute band liquation depends primarily on the temperature gradient in the vicinity of the weld interface and on the extent of solute segregation. In addition to partial melting, areas adjacent to the weld interface experience austenite grain growth. As austenite grains grow, their boundaries impinge upon liquated regions and are wet by the liquid. This wetting pins austenite grain boundaries and prevents further grain boundary migration.

If liquated regions are sufficiently high in ferritizers, or low in austenitizers, subsequent solidification occurs as primary ferrite, and results in the continued pinning of austenite grain boundaries during weldment cooling. The enrichment of ferritizers and the rapid cooling rates present in the partially-melted region prevent this ferrite from transforming entirely to austenite on cooling and result in the retention of some ferrite to room temperature.

Studies by Dudley[6] found that the rapid heating rates which characterize the weld-interface region can induce dissolution of niobium carbides in Type 347 stainless steel (Nb-stabilized) by a constitutional liquation phenomenon. This phenomenon, which has been observed in several additional alloy systems,[1,7] may also promote liquation along solute bands and grain boundaries in the partially-melted region of weldments on Type 304 base materials.

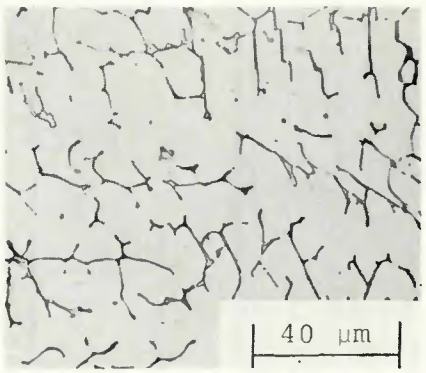

Fig. 3—Duplex austenite-ferrite microstructure of typical 18Cr-8Ni autogenous weldment. Dark-etching ferrite is present at the core of the originally-solidified primary ferrite dendrites. Mixed acid etch, ×500

During welding, base metal regions adjacent to the weld interface experience very rapid heating rates. This rapid heating can result in the dissolution of chromium carbides present in solute bands and at austenite grain boundaries, and provide a subsequent enrichment of carbon and chromium in the austenite which originally bounded the carbide particles. Local increases in the carbon content lower the effective melting temperature of these regions and promote liquation.

The large carbon and chromium compositional gradients, which exist between the liquated areas and surrounding austenite, result in the diffusion of these elements into the austenite. Interstitial diffusion of carbon proceeds at a rate several orders of magnitude greater than substitutional diffusion of chromium. For this reason, the chromium-to-carbon ratio in the liquid increases. This increase results in the ultimate solidification of this region as primary ferrite rather than austenite. The rapid cooling rates present in the partially-melted region prevent this ferrite from transforming entirely to austenite on cooling and results in the retention of some ferrite to room temperature. It is important to note that these constitutionally-liquated and subsequently ferritic regions interact with growing austenite grains in a manner identical to that described previously, despite differences in the mechanism of liquation.

Fig. 4—Macrograph of a Type 312/Type 304L GMAW-P weldment. Mixed acid etch, ×20 (reduced 50% on reproduction)

The "True" Heat-Affected Zone

Ferrite may also be formed in the "true" weld heat-affected zone (HAZ). During welding, the austenitic base metal surrounding melted and partially-melted regions is rapidly heated to temperatures in the two phase austenite plus ferrite region (Fig. 2) where a solid-state transformation from austenite to ferrite can occur.

Regions which transform to ferrite on heating are usually solute bands (oriented parallel to the plate or sheet rolling direction) where ferrite-stabilizing elements are highly concentrated, or where austenite-stabilizing elements are in low concentration. Electron-microprobe studies performed by Matsuda[8] have shown that at high temperatures ferrite-stabilizing elements exhibit a greater solubility in ferrite than in austenite, and consequently partition to the ferrite. Likewise, austenite-stabilizing elements are more soluble in austenite than in ferrite and tend to partition to the austenite. The rapid cooling rates present in the HAZ, coupled with alloying-element partitioning, prevent the ferritic areas from transforming entirely back to austenite on cooling; this results in the retention of some ferrite to room temperature.

The amount and distribution of ferrite in the "true" HAZ depend on several factors. Studies undertaken by Williams[9] on heat-affected zone formation during the flash-butt welding of Type 321 austenitic stainless steel recognized the importance of base metal composition, structure, homogeneity, maximum temperature, and cooling rate in determining HAZ ferrite morphology. HAZ simulation studies on Type 304 stainless steel by Hines[10] and Sherman[1] further illustrated the importance of maximum temperature, time at temperature, and cooling rate in controlling both the amount of HAZ ferrite and the ferrite morphology.

Experimental Procedures

Materials

Single-pass weldments were produced on hot-rolled, wholly-austenitic 0.107 in. (2.72 mm) thick Type 304L stainless steel sheet using the pulsed gas-metal arc (GMAW-P) welding process. Types 310 and 312 stainless steel filler metal wires were employed to produce composite regions with wholly-austenitic and 30 vol-% ferrite, respectively. As illustrated in Fig. 4, weldments were full-penetration and exhibited considerable reinforcement.

Table 1—Chemical Compositions of Stainless Steel Base and Filler Materials, Wt-%

	Type 304L	Type 310	Type 312
Carbon	0.037	0.11	0.12
Chromium	18.55	27.11	28.79
Nickel	9.61	21.11	8.68
Manganese	1.55	1.65	1.58
Silicon	0.59	0.47	0.50
Molybdenum	0.18	0.07	0.13
Sulfur	0.005	0.002	0.013
Phosphorus	0.031	0.014	0.020

Table 2—Welding Parameters for GMAW-P Weldments

Welding current avg	140 A
Arc voltage	24 V, DCSP
Pulse frequency	120 cycles/s
Travel speed	10 ipm
Wire feed speed	280 ipm
Electrode type	0.045 in. (1.14 mm) diameter solid wire
Electrode extension	0.66 in. (16.8 mm) from contact tip
Shielding gas	argon + 2% oxygen, 40 cfh (18.9 liters/min.)

Chemical compositions of the base and filler metals are provided in Table 1. Table 2 summarizes welding parameters and conditions employed in weldment fabrication.

Microprobe Analysis

Specimens selected for electron probe microanalysis (EPMA) were sectioned transverse to the welding direction, mechanically polished, and etched to reveal the desired microstructure. Microhardness marks were employed to identify specific areas and the specimen was repolished in preparation for EPMA.

Analysis was performed using a point-count technique with an accelerating voltage of 20 kV and a nominal specimen current of 0.25 μA. The spatial resolution of the electron beam was on the order of 10 μM. The X-ray intensity data collected at specific points was corrected for atomic number, absorption, fluorescence and backscatter errors, and converted to weight percents using the Magic IV computer program.[11]

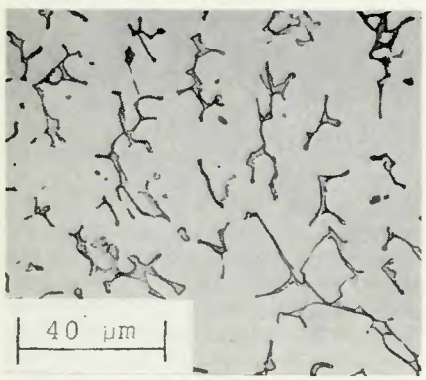

Fig. 6—Duplex austenite-ferrite microstructure typical of the unmixed zone in Type 310/Type 304L weldment. Mixed acid etch, ×500

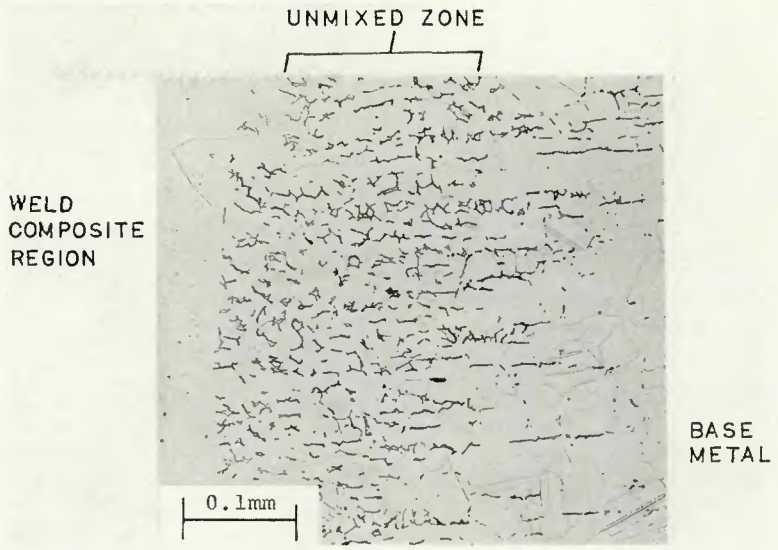

Fig. 5—Fusion boundary region of a Type 310/Type 304L GMAW-P weldment. Mixed acid etch, ×200

Stress Corrosion Cracking Testing

Constant extension rate SCC tests (also described as constant strain rate or constant deflection rate tests) were performed on tensile specimens which contained a single-pass GMAW-P weldment transverse to the longitudinal axis. Tests were conducted in room and elevated-temperature chloride-containing solutions which readily produce SCC in stressed 18Cr-8Ni stainless steels.

Smooth-surfaced tensile specimens were machined from welded sheet materials such that the gage-section weldment was coincident with the center of the weldment length. This procedure assured that the macrosegregation associated with the solute transients in the initial and final regions of solidification was not present in the test specimens; it also provided a consistent gage-section weldment ferrite morphology and content. Subsequent to machining (which included removal of the weld reinforcement), the specimen was dry-ground to nominal size and wet-ground to a 600 grit finish. The final grinding direction was parallel to the longitudinal axis of the specimen.

Room and elevated temperature SCC tests were conducted in a transparent Pyrex cell. Loads were applied

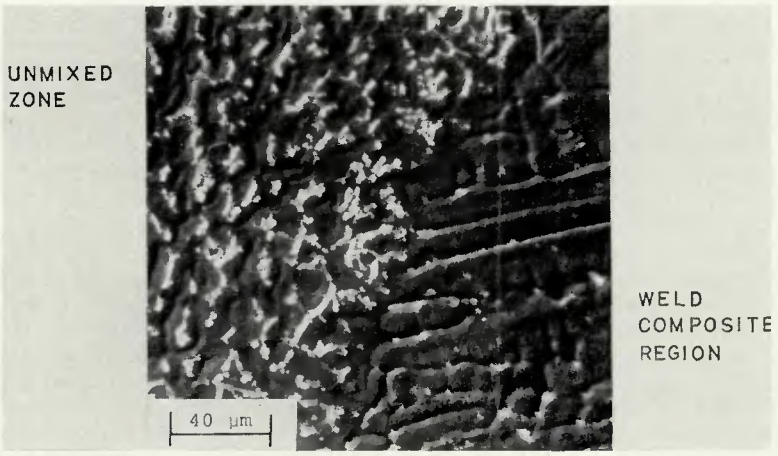

Fig. 7—Nomarski micrograph of Type 310/Type 304L GMAW-P weldment fusion boundary region. Retained delta ferrite present in the unmixed zone appears as white "ridges," while the last-to-solidify cellular-dendrite boundaries are the dark "valleys." Some ferrite is evident along primary austenite cell boundaries in the composite region

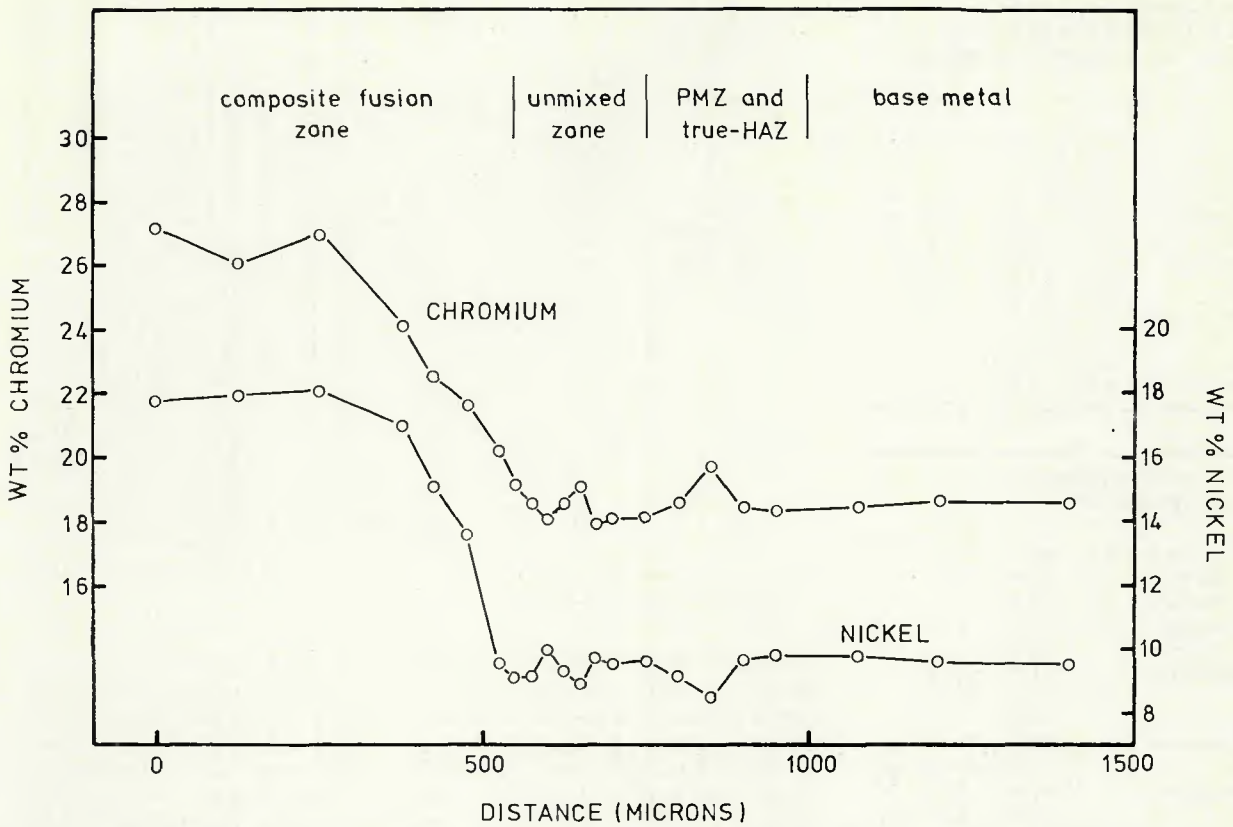

Fig. 8—Concentration profile of chromium and nickel across the weld fusion boundary region of a Type 310/Type 304L GMAW-P weldment

at a constant extension rate by a conventional Instron testing machine and monitored continuously on a strip chart recorder. Room-temperature tests were performed in 1*N* HCl, 5*N* H_2SO_4 + 0.5*N* NaCl, and 5*N* H_2SO_4 + 1*N* NaCl at 23 ± 2 C (73 ± 4 F). Solutions were prepared from reagent grade concentrated solutions and chemicals, and continuously dearated during testing by bubbling high-purity argon through the test cell.

Wholly-austenitic and high-ferrite transverse-welded specimens were tested in the room temperature solutions at an extension rate of 5.08×10^{-5} cm/min (2×10^{-5} ipm) (equivalent to an initial strain rate of 1.48×10^{-6} s^{-1}) and in air at an extension rate of 5.08×10^{-4} cm/min (2×10^{-4} ipm) (equivalent to an initial strain rate of 1.48×10^{-5} s^{-1}).

Elevated temperature tests were performed in 38 and 42 wt-% boiling $MgCl_2$ at 135 and 154 C (275 and 309 F), respectively. Solution temperature and concentration were maintained constant by an immersion heater-reflux condenser system. $MgCl_2$ test solutions were prepared from reagent grade hydrous $MgCl_2$ crystals ($MgCl_2 \cdot 6H_2O$) and distilled water in a manner recommended by ASTM Standard G36-73.[12] Wholly-austenitic and high-ferrite transverse-welded specimens were tested in the $MgCl_2$ solutions and in liquid paraffin (154 C, i.e. 309 F) at an extension rate of 5.08×10^{-4} cm/min (equivalent to an initial strain rate of 1.48×10^{-5} s^{-1}).

Results and Discussion

Unmixed Zone Morphology and Formation

Figure 5 illustrates the fusion boundary region of the Type 310/Type 304L GMAW-P weldment, which exhibits wholly-austenitic composite and unaffected base metal regions. Ferrite formation along solute bands in the "true" heat-affected zone and at grain boundaries and solute bands in the partially-melted region is clearly apparent. In addition, the presence of a large, duplex unmixed zone is evident. As Fig. 6 illustrates, the unmixed zone appears morphologically similar to the fusion zone of an autogenous 18Cr-8Ni stainless steel weldment (Fig. 3), with semi-continuous ferrite present in a vermicular microstructure.

Solidification of the unmixed zone initiates epitaxially on ferritic areas in the partially-melted region and proceeds in a manner identical to that observed in the 18Cr-8Ni weldment fusion zone. The Nomarski interference micrograph in Fig. 7 shows that ferrite is retained to room temperature at the cores of originally-solidified primary-ferrite dendrites.

Last-to-solidify cellular-dendrite boundaries in the unmixed zone and cell boundaries in the wholly-austenitic composite region are quite distinguishable from the ferrite present at cellular-dendrite cores in the unmixed zone. At the unmixed zone—composite region boundary a transition from primary-ferrite to primary-austenite solidification occurs, with the primary austenite solidifying epitaxially on austenitic regions in the unmixed zone.

The existence of an unmixed zone in Type 310/Type 304L weldments was also confirmed by EPMA studies. Chromium and nickel contents across the weld fusion boundary region are shown in Fig. 8 and indicate that the mean chemical composition of the unmixed zone is virtually identical to that of the unaffected base metal. Local variations in Cr and Ni contents within the unmixed zone, the partially-melted region, and the "true" heat-affected zone result from localized microstructural variations in these duplex regions (e.g., high Cr and low Ni contents are observed if the electron beam was located on a predominantly ferritic region).

As Fig. 9 illustrates, a duplex unmixed zone is also present in the high-ferrite, Type 312/Type 304L weldment. As in the Type 310/Type 304L weldment, primary-ferrite solidification in the unmixed zone occurs epitaxially on ferritic areas in the partially-melted region. At the unmixed zone-composite region boundary, solidification of the composite region initiates as a continued growth

of delta ferrite present in the unmixed zone. Mean chromium and nickel contents in the unmixed zone were found to be comparable to those of the Type 304L base metal.

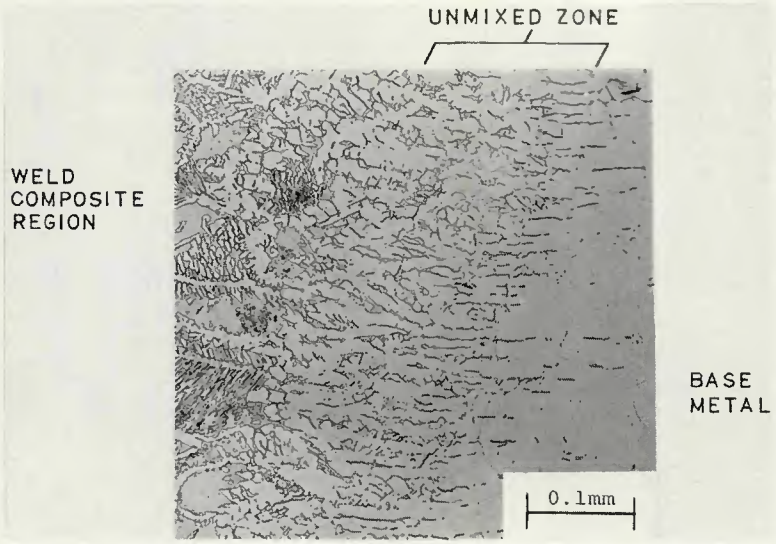

Fig. 9—Fusion boundary region of a Type 312/Type 304L GMAW-P weldment. Mixed acid etch, ×200

Table 3—Results of Constant Extension Rate SCC Tests Performed on Transverse-Welded Specimens

Weldment	Test Environment	Test Temperature, C	Initial strain rate (sec^{-1})	Maximum engineering stress, ksi	Failure location[a]
Type 310/ Type 304L	Air	23	1.48×10^{-5}	78	WCR
	1*N* HCl	23	1.48×10^{-6}	69	WCR/HAZ
	5*N* H_2SO_4 + 1*N* NaCl	23	1.48×10^{-6}	53	WCR/HAZ
	5*N* H_2SO_4 + 0.5*N* NaCl	23	1.48×10^{-6}	56	WCR/HAZ
	44wt-% $MgCl_2$	154	1.48×10^{-5}	32	BM
	38wt-% $MgCl_2$	135	1.48×10^{-5}	39	BM
	Liquid paraffin	154	1.48×10^{-5}	65	BM
Type 312/ Type 304L	Air	23	1.48×10^{-5}	90	BM
	1*N* HCl	23	1.48×10^{-6}	62	HAZ/BM
	5*N* H_2SO_4 + 1*N* NaCl	23	1.48×10^{-6}	51	WCR
	5*N* H_2SO_4 + 0.5*N* NaCl	23	1.48×10^{-6}	50	WCR
	44wt% $MgCl_2$	154	1.48×10^{-5}	34	BM
	38wt%, $MgCl_2$	135	1.48×10^{-5}	39	BM
	Liquid paraffin	154	1.48×10^{-5}	65	BM

[a]BM—base metal; WCR—weldment composite region; HAZ—heat-affected zone.

The formation of quite sizable unmixed zones in both the "high-ferrite" and "wholly-austenitic" GMAW-P weldments is a somewhat unexpected phenomenon, since one might normally expect hydrodynamic mixing in the composite region to eliminate such a possibility. Evidently, the dynamic characteristics of fluid flow in the weldments are such that large regions of the base metal are allowed to melt, remain relatively stagnant, and resolidify. Thus, these heterogeneous weldments essentially consist of a composite region bounded by an 18Cr-8Ni "autogenous weldment."

Stress-Corrosion Cracking Properties

Table 3 summarizes the results of constant extension rate and stress-corrosion cracking tests performed on transverse-welded specimens in chloride-containing solutions which produce stress-corrosion cracking in 18Cr-8Ni stainless steel base metals. Values of maximum engineering stress for specimens tested in corrosive and neutral environments, and scanning-electron microscopy studies provide a basic means of comparing the susceptibility of specimens to stress-corrosion cracking under constant extension rate conditions.

Room-Temperature Testing

Type 310/Type 304L Weldments. Failure of transverse-welded specimens which exhibit wholly-austenitic base and weld metals tested in low-pH, room-temperature solutions occurs as a combination of environmentally-induced attack in the unmixed zone and ductile failure in the weldment composite region. The severity of this preferential attack is illustrated in Fig. 10 for a specimen tested in a 5*N* H_2SO_4 + 1*N* NaCl solution.

Specimens tested in 1*N* HCl and the H_2SO_4 + NaCl solutions appear macroscopically and microscopically very

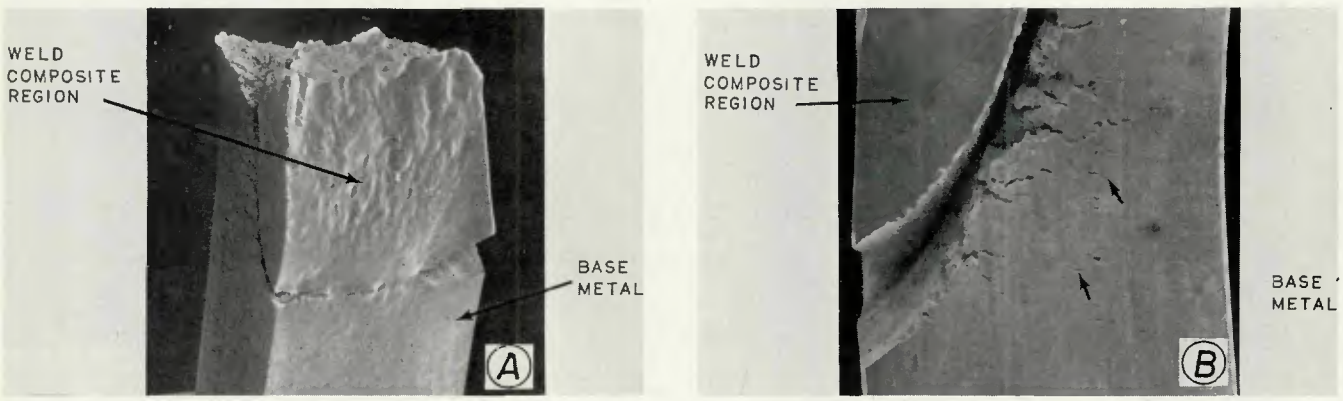

Fig. 10—SEM macrographs of Type 310/Type 304L transverse-welded specimens tested under CER conditions in 5N H_2SO_4 + 0.5 N NaCl. ×20. A—note the preferential attack at the fusion boundary region, ×20; B— arrows show transgranular SCC in the base metal, ×40 (A and B reduced 41% on reproduction)

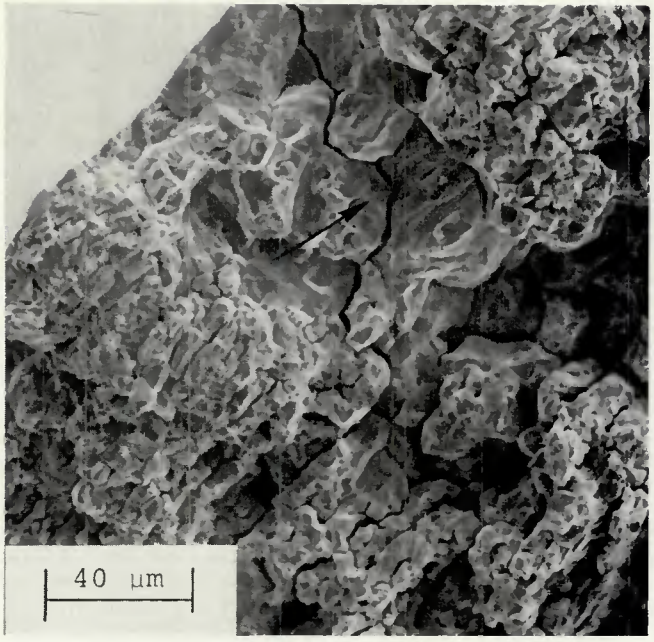

Fig. 11—SEM fractrograph of a Type 310/Type 304L transverse-welded specimen tested under CER conditions in 5N H_2SO_4 + 0.5 N NaCl. Arrow indicates possible dissolution in the partially-melted region. ×500

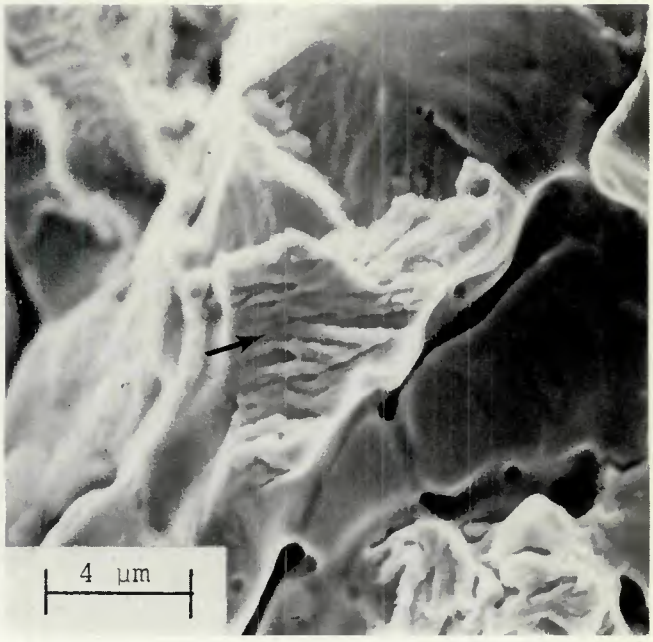

Fig. 12—SEM fractrograph of a Type 310/Type 304L transverse-welded specimen tested under CER conditions in 5N H_2SO_4 + 0.5N NaCl. Arrow shows region of transgranular SCC in the austenite. ×5000

similar. Lower values of maximum engineering stress and greater depths of attack in specimens tested in H_2SO_4 + NaCl, compared to those tested in 1*N* HCl, suggest that the H_2SO_4 + NaCl solutions are more aggressive.

Unmixed zone attack occurs by a combination of stress-assisted ferrite dissolution and stress-corrosion cracking in the austenite. The cellular-dendritic nature of the duplex unmixed zone is apparent from the SEM fractograph shown in Fig. 11. Evidence that attack may occasionally proceed along ferrite-covered base metal austenite grain boundaries in the partially-melted region is also presented in Fig. 11. Areas of transgranular stress-corrosion cracking in the austenite are observable on the fracture surfaces. The SEM fractograph in Fig. 12, which shows the fracture surface area in Fig. 11 at a high magnification, indicates that transgranular stress corrosion cracking of the austenite may occur by a tunneling mechanism identical to that observed by Scully[13] in a similar alloy-environmental system.

Transgranular stress-corrosion cracking in unaffected base metal regions of these specimens can also be found, particularly in regions adjacent to the fusion zone. This stress-corrosion cracking does not, however, appear to influence specimen failure. Despite considerable plastic deformation, stress-corrosion cracking in the wholly-austenitic weldment composite region does not occur.

Type 312/Type 304L Weldments. Failure of transverse-welded specimens which contain a high-ferrite weldment composite region tested in low-pH, room-temperature solutions depends on the aggressiveness of the solution. In mildly-aggressive 1*N* HCl failure occurs by a combinaton of

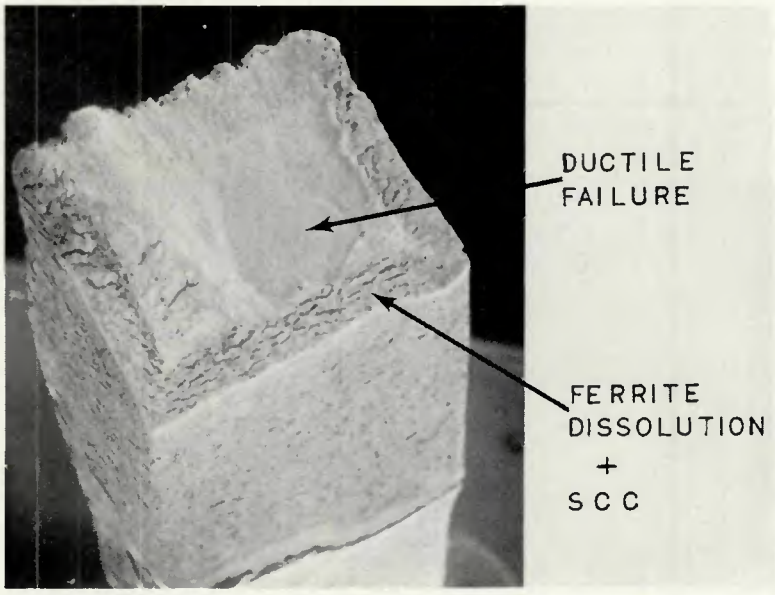

Fig. 13—SEM macrograph of a Type 312/Type 304L transverse-welded specimen tested under CER conditions in 1N HCl. (reduced 11.8% on reproduction) ×20

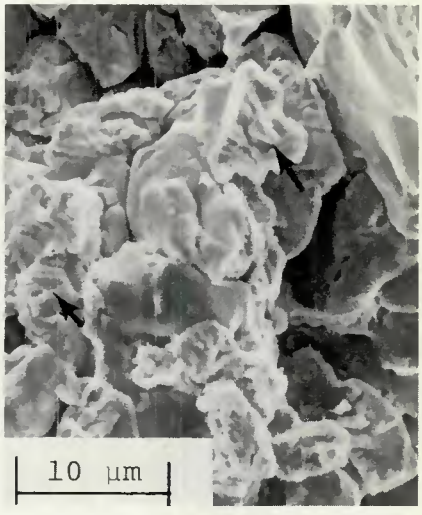

Fig. 14—SEM fractrograph of a Type 312/Type 304L transverse-welded specimen tested under CER conditions in 1N HCl. Arrows indicate regions of transgranular SCC in the austenite. ×2000

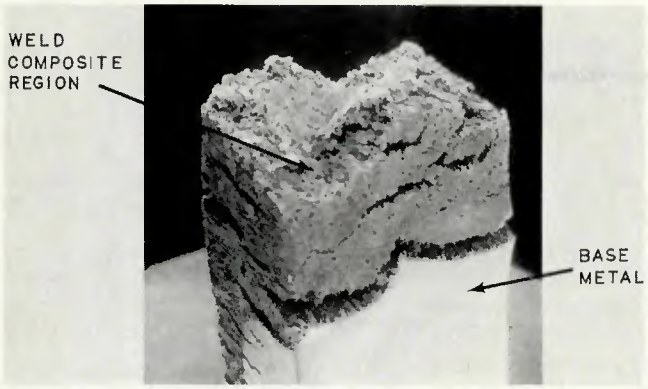

Fig. 15—SEM macrograph of Type 312/Type 304L transverse-welded specimen tested under CER conditions in 5N H_2SO_4 + 1N NaCl. ×20 (reduced 41% on reproduction)

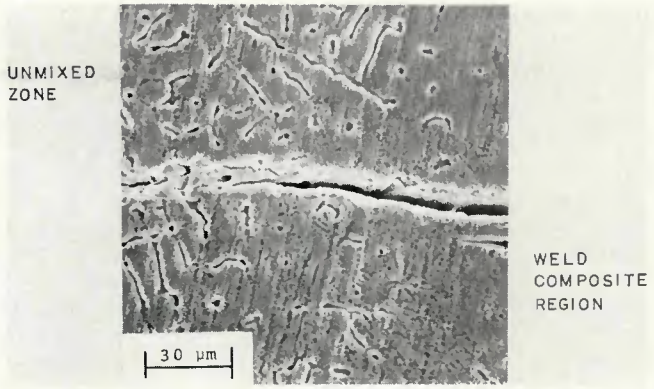

Fig. 16—SEM micrograph of a Type 310/Type 304L transverse-welded specimen tested under CER conditions in boiling $MgCl_2$ at 154 C (309 F). Ferrite is etched in the unmixed zone. Marble's etch, ×1500

environmentally-induced attack and ductile failure in the weld fusion boundary region—Fig. 13.

The SEM fractograph illustrated in Fig. 14 provides evidence that unmixed zone and partially-melted region attack occurs in a manner identical to that observed in wholly-austenitic weldments described in the previous section. These similarities are also indicated by the identical values of maximum engineering stress for wholly-austenitic and high-ferrite transverse-welded specimens tested in 1*N* HCl. Transgranular stress-corrosion cracking in the unaffected base metal and ferrite dissolution in the high-ferrite weldment composite region are also observed in specimens tested in 1*N* HCl. However, these phenomena do not appear to directly influence specimen failure.

Failure of specimens tested in the aggressive H_2SO_4 + NaCl solutions occurs in the weldment composite region by a combination of ferrite dissolution and ductile failure. As Fig. 15 shows, considerable fusion line attack is also apparent in these specimens. This attack occurs predominantly in the unmixed zone by the ferrite dissolution/stress-corrosion cracking process described previously.

Elevated-Temperature Testing

Type 310/Type 304L Weldments. Failure of transverse-welded specimens which exhibit wholly-austenitic base and weld metals tested in boiling $MgCl_2$ occurs as a combination of stress-corrosion cracking and ductile failure in the unaffected base metal remote from the weldment composite region. Stress-corrosion cracks in the base metal of specimens tested at 154 C (309 F) proceed in transgranular or mixed transgranular/intergranular modes. At 135 C (275 F) stress-corrosion cracks propagate almost entirely by an intergranular mode.

Specimens tested at 154 C (309 F) also exhibit numerous small stress-corrosion cracks in the unmixed zone and the weldment composite region at the root of the weldment. The SEM micrograph in Fig. 16 shows stress-corrosion cracks that propagate in both the duplex unmixed zone and the wholly-austenitic weldment composite region. Stress-corrosion cracking appears to occur transgranularly in the composite region and by a mixed transgranular/interphase-interface mode in the unmixed zone. Composite region failure of specimens tested in liquid paraffin indicates that the composite region deforms plastically more readily than both the fusion boundary region and the unaffected base metal.

Greater resistance to stress-corrosion cracking in $MgCl_2$ of Type 310 stainless steel, compared to Type 304 materials, has been shown by Denard[14] and accounts for the minimal cracking present in the composite region despite its lower strength. The nature of the weldment geometry (Fig. 4) and the low strength of the weldment composite region result in locally high strain rates (prior to crack initiation) in the unmixed zone at the root of the weldment. This increased strain rate induces preferential attack in this region of the weldment.

Type 312/Type 304L Weldments. Failure in transverse-welded specimens which exhibit a high-ferrite weldment composite region occurs in the base metal remote from the weldment composite region in a manner similar to that described previously for Type 310/Type 304L specimens. Specimens tested at 154 C (309 F) also exhibited preferential attack at the weld interface near the toe of the weldment—Fig. 17.

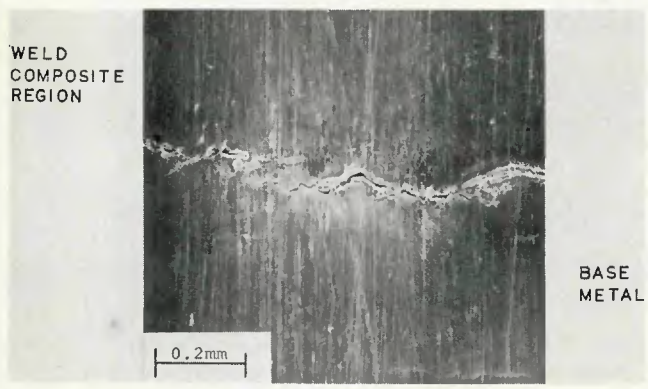

Fig. 17—SEM macrograph of a Type 312/Type 304L transverse-welded specimen tested under CER conditions in boiling $MgCl_2$ at 154 C. ×100

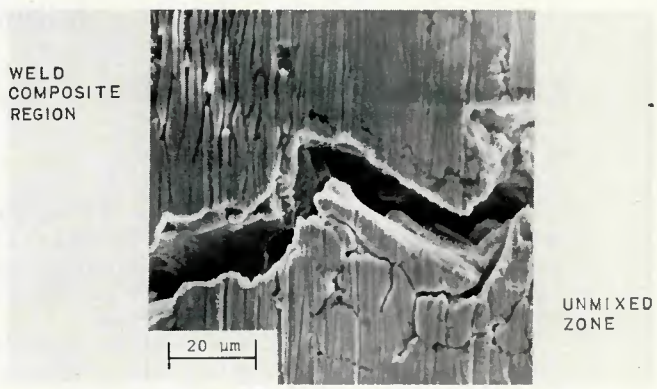

Fig. 18—SEM micrograph of a Type 312/Type 304L transverse-welded specimen tested under CER conditions in boiling $MgCl_2$ at 154 C (309 F). ×1000

The SEM micrograph in Fig. 18 indicates that stress-corrosion cracking and ferrite dissolution in the vicinity of cracks occurs at the unmixed zone-weldment composite region boundary. Stress-corrosion cracks appear to propagate predominantly in the unmixed zone. Failure in the unaffected base metal of specimens tested in liquid paraffin at 154 C (309 F) indicates that the weldment composite region and the fusion boundary region exhibit greater strengths than the unaffected base metal. Preferential attack in the unmixed zone at the weldment toe may result from the geometry of the weldment; this places the unmixed zone at the weldment toe in a region which experiences a strain rate (prior to crack initiation) equivalent to that present in the weaker unaffected base metal.

Conclusions

The following conclusions pertain to unmixed zone formation and morphology in heterogeneous weldments on wholly-austenitic Type 304L stainless steel:

1. Unmixed zone formation occurs readily in GMAW-P weldments, regardless of the chemical composition and microstructural characteristics of the weldment composite region.

2. The unmixed zone microstructure appears morphologically similar to that of an autogenous weld metal in 18Cr-8Ni stainless steel, with semicontinuous ferrite present in a vermicular morphology.

3. Solidification of the unmixed zone occurs epitaxially on ferritic regions in the partially-melted region and proceeds by a manner identical to that observed in 18Cr-8Ni weld metals.

The following conclusions pertain to stress-corrosion cracking studies on transverse-welded specimens tested under constant-extension rate conditions in room and elevated-temperature solutions:

1. The duplex unmixed zone in weldments exhibiting either wholly-austenitic or high-ferrite composite regions is highly susceptible to attack in low-pH, room-temperature solutions by the simultaneous and complementary occurrence of stress-corrosion cracking in the austenite and stress-assisted ferrite dissolution.

2. Failure of transverse-welded specimens in $MgCl_2$ solutions occurs in the base metal remote from the weldment. However, preferential attack in the unmixed zone of both the wholly-austenitic and high-ferrite weldments at 154 C (309 F) is evident.

Acknowledgment

The authors would like to acknowledge both the Department of Energy (Contract No. EY-76-5-02-2462*000.) and Chemetron Corporation for providing finanical support for this investigation.

References

1. Savage, W. F., Nippes, E. F., and Szekeres, E. S., "A Study of Weld Interface Phenomena in a Low Alloy Steel," *Welding Journal,* 55(9), Sept. 1976, Research Suppl., pp. 260-s to 268-s.

2. Masumoto, I., Tamaki, K., and Katusuna, M., "Hot Cracking of Stainless Steel," *J. Japan Welding Society,* 41(11), Nov. 1972, pp. 1306-1314.

3. Savage, W. F., Baeslack, W. A., and Lippold, J. C., Unpublished research performed at Rensselaer Polytechnic Institute, Troy, New York, 1977.

4. Sherman, D. H., "The Corrosion and Stress Corrosion Cracking Behavior of Stainless Steel Weldments Containing Ferrite," Doctor's Thesis, Rensselaer Polytechnic Institute, Troy, New York, 1973.

5. Savage, W. F., Nippes, E. F., and Miller, T. W., "Microsegregation in Partially-Melted Regions of 70 Cu-30Ni Weldments, *Welding Journal,* 55(7), July, 1976, Research Suppl., pp. 181-s to 187-s.

6. Dudley, R. H., "An Experimental Investigation of the Constitutional Liquation Hypothesis," A Doctor's Thesis, Rensselaer Polytechnic Institute, Troy, New York, 1962.

7. Aronson, A. H., "Constitutional Liquation in a Plain Carbon, High-Carbon Steel," A Master's Thesis, Rensselaer Polytechnic Institute, Troy, New York, 1963.

8. Arata, Y., Matsuda, F. and Katayma, S., "Solidification Crack Susceptibility in Weld Metals of Fully-Austenitic Stainless Steels (Report I)—A Fundamental Investigation of Solidification Behavior of Fully-Austenitic and Duplex Microstructures and the Effect of Ferrite on Microsegregation," *Transactions of the JWRI,* 5(2), Feb., 1976, pp. 142-143.

9. Williams, N. T., "Influence of Welding Cycles on the Ferrite Content of Type 321 Austenitic Steel," *British Welding Journal,* Sept. 1965, pp. 435-441.

10. Hines, R. B., "An Investigation of Microsegregation and Morphology of Delta Ferrite in Type 304 Stainless Steel," A Master's Thesis, Rensselaer Polytechnic Institute, Troy, New York, 1975.

11. Colby, J. W., *Magic IV Computer Program,* Bell Telephone Laboratories, Allentown, Pa.

12. "Performing Stress-Corrosion Cracking Tests in a Boiling Magnesium Chloride Solution," ASTM Standard G36-73, ASTM, 1973.

13. Scully, J. C., "Fractographic Aspects of Stress-Corrosion Cracking," *The Theory of Stress Corrosion Cracking in Alloys,* NATO, Brussels, 1971, pp. 127-166.

14. Denard, E. E., "Effect of Composition and Heat Treatment on the Stress Corrosion Cracking of Austenitic Stainless Steels," *Corrosion,* 16(7), July 1960, p. 359t.